Effect of Precursor Core Structure on the Hydrogenation of 1,3-Butadiene Catalyzed by Cluster-Derived Model Catalysts

Miguel A. Bañares,[†] Laurent Dauphin,[‡] Xinjian Lei,[‡] Wei Cen,[‡] Maoyu Shang,[‡] Eduardo E. Wolf,*[,†] and Thomas P. Fehlner*[,‡]

Department of Chemical Engineering and Department of Chemistry and Biochemistry, University of Notre Dame, Notre Dame, Indiana 46556

Received October 6, 1994. Revised Manuscript Received December 15, 1994[⊗]

The cobalt–carbonyl cluster ligand based complexes, $M_2\{\mu\text{-}[(CO)_9Co_3(\mu_3\text{-}CCO_2)]\}_4$, M = Mo, Cu, were converted into active solids by thermolysis. These precursor complexes contain a square planar array of tricobalt clusters centered by a M_2 carboxylate bridged core which is M–M bonding in the case of M = Mo and nonbonding in the case of M = Cu. TGA, TPD-MS, XPS, BET, and in situ DRIFTS measurements demonstrate the existence of two forms of the resulting materials as well as differences in these materials due to precursor structure. The first, formed at 400 K, is designated LT-MCo, M = Mo, Cu, and results from partial decarbonylation of the precursor with retention of metal carboxylate linkages. The second, formed at 500 K is designated HT-MCo and results from the full decarbonylation of the precursor and, under H_2, full decarboxylation. The catalytic activity of these materials for the hydrogenation of 1,3-butadiene was studied. Significant differences in the activities and selectivities for the LT- and HT-MCo materials are observed and demonstrate a dependence of catalytic behavior on molecular precursor core structure.

Introduction

The use of organometallic clusters to prepare small catalyst particles is a well-known approach in catalysis.[1,2] These materials often lose their integrity upon activation or interaction with the support and, consequently, the role of the cluster structure itself is not very clear.[3,4] Recently we have described the preparation of high surface area metallic solids from the thermolysis of coordination compounds with multinuclear transition metal cluster substituents ("clusters of clusters").[5] That is, $Co_4O[(CO)_9Co_3CCO_2]_6$ and $Zn_4O[(CO)_9Co_3CCO_2]_6$ (Chart 1a) are converted on heating into high surface area amorphous solids designated CoCo and ZnCo, respectively. The catalytic properties of these materials toward the hydrogenation of 1,3-butadiene has been described previously.[6,7] In essence the studies showed that these materials are active catalysts with selectivities that differ from catalysts derived from transition-metal clusters alone or from conventional supported metal catalysts. Importantly, activities and selectivities depend on precursor composition and structure as well as preparation temperature and conditions.

Chart 1

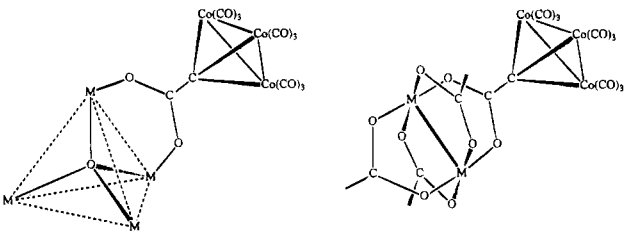

These cluster-substituted coordination compounds degrade on heating, and the resulting solids possess microstructures that are related to the complex precursor molecules. That is, our interpretation of the available data on the amorphous, porous solids CoCo and ZnCo suggests that loss of CO ligands from the cobalt clusters results in intercluster bond formation. These interactions, plus retention of some carboxylate links, give rise to a regular porous network with cobalt metal exposed to the void volume. Further heating results in CO_2 formation and the loss of the carboxylate links in the core structure of the precursor. The hydrogenation of 1,3-butadiene was used to further characterize these novel materials, i.e., the catalysis of the reaction was considered a probe of the materials rather than the materials being considered as new olefin hydrogenation catalysts. Thus, it was shown that both activities and selectivities depend on the nature of the cluster of clusters precursor used. However, the connection between materials properties, particularly catalytic properties, is not yet clear.

One of the advantages of this precursor approach is that a large variety of cluster of clusters geometries can be contemplated and synthesized. Thus, we report the synthesis of two clusters of clusters with square planar

⊗ Abstract published in *Advance ACS Abstracts,* February 1, 1995.

(1) *Studies in Surface Science and Catalysis*; Gates, B., Guczi, L., H., K., Eds.; Elsevier: New York, 1986; Vol. 29.
(2) Iwasawa, Y. *Tailored Metal Catalysts*; Reidel: Hingham, MA, 1986.
(3) Primet, M.; El Azahar, M.; Guenin, M. *Appl. Catal.* **1993**, *58*, 241.
(4) Tardy, B.; Noupac, C.; Leclerk, C.; Bertolini, J. C.; Hoareau, A.; Treilleux, M.; Fanre, J. P.; Nohoul, G. *J. Catal.* **1991**, *129*, 1.
(5) Cen, W.; Ladna, B.; Fehlner, T. P.; Miller, A. E.; Yue, D. *J. Organomet. Chem.* **1993**, *449*, 19.
(6) Kalenik, Z.; Ladna, B.; Wolf, E. E.; Fehlner, T. P. *Chem. Mater.* **1993**, *5*, 1247.
(7) Bañares, M.; Dauphin, L.; Calvo-Pérez, V.; Fehlner, T. P.; Wolf, E. E. *J. Catal.*, in press.

0897-4756/95/2807-0553$09.00/0

tricobalt cluster arrays (Chart 1b), $Mo_2\{\mu$-$[(CO)_9Co_3(\mu_3$-$CCO_2)]\}_4$[8] and $Cu_2\{\mu$-$[(CO)_9Co_3(\mu_3$-$CCO_2)]\}_4$, the conversion of these precursors into active solids, MoCo and CuCo, respectively, and the behavior of these solids as catalysts in the hydrogenation of 1,3-butadiene.

The primary objective of this study was to investigate the role of the cluster core in determining materials properties. First, we are interested in any effects of the spatial orientation of the tricobalt clusters on the initial intercluster bond formation. X-ray crystallographic studies show that the CoCo and ZnCo precursors have an octahedral arrangement of the tricobalt clusters determined by their coordination to the six edges of the M_4-oxo cores (Chart 1a). The new compounds have square planar cluster arrays (Chart 1b). Second, we know that in order to generate active materials, the links to the inner core must be retained during decarbonylation of the outer metal clusters.[9] However, the role of the inner core bonding itself is not clear. The CoCo and ZnCo precursors have centered oxygen atoms with strong M−O bonds (Chart 1a). On the other hand, while $Mo_2\{\mu$-$[(CO)_9Co_3(\mu_3$-$CCO_2)]\}_4$ possesses a quadruply bonded metal core, the copper centers in $Cu_2\{\mu$-$[(CO)_9Co_3(\mu_3$-$CCO_2)]\}_4$ are essentially nonbonded. Therefore, these two compounds permit an examination of the importance of core bonding. Finally, of course, the different core metals themselves may play a role in the catalytic reaction.

Experimental Section

Precursor Synthesis. $Mo_2\{\mu$-$[(CO)_9Co_3(\mu_3$-$CCO_2)]\}_3$-$[\mu$-$(CH_3CO_2)]$·$C_6H_5CH_3$: Freshly prepared crystalline $(CO)_9Co_3$-$(\mu_3$-$CCOOH)$[10] (0.486 g, 1.00 mmol) and $Mo_2(CH_3CO_2)_4$ (0.214 g, 0.5 mmol) were loaded into a 250 mL Schlenk flask equipped with a capping rubber septum and a magnetic stirring bar. This flask had been evacuated and refilled with N_2 several times before THF (40 mL) was added to the flask via syringe with rapid stirring. The reaction mixture quickly turned purple then to a midnight blue color within 1 min at room temperature. Another 7 min was sufficient to complete the reaction which was monitored by TLC and solution IR spectroscopy. As a consequence, TLC (toluene) showed a major intense blue band at $R_f = 0.8$, together with a very pale purple spot at $R_f = 0.4$ and a pale yellow-brown spot at $R_f = 0.0$. THF was removed under vacuum and the residual solid material was extracted with 5 × 15 mL toluene. The extract was quickly filtered through a 3 cm degassed silica gel bed, giving a pure compound with a single spot at $R_f = 0.8$ in TLC (toluene). Black-blue needlelike crystals were obtained as the filtrate was slowly pumped to dryness. These were characterized as $Mo_2\{\mu$-$[(CO)_9Co_3(\mu_3$-$CO_2)]_3[\mu$-$(CH_3CO_2)]$·$C_6H_5CH_3$ (0.450 g, 0.24 mmol). The yield based on total cobalt is 73%. Anal. Calcd for $Mo_2Co_9C_{42}O_{35}H_{11}$: Co, 29.50; Mo, 10.67; C, 28.06; H, 0.61. Found: Co, 29.20; Mo, 10.10; C, 27.94; H, <0.5. MS (+FAB) (M) 1705.7. IR (KBr, cm^{-1}, carbonyl and carboxylate regions) 2106 s, 2052 vs, br, 2048 vs, br, 1518 w, 1494 w, 1439 m, 1366 m. ^1H NMR (300 MHz, CD_2Cl_2; 20 °C; d) 2.34 (s, 3H), 2.59 (s, 3H), 7.20 (m, 5H) arising from one acetate and a solvate toluene. $^{13}C\{^1H\}$ NMR (CD_2Cl_2; 20 °C; d) 199.6, 21.4, 1.4.

$Mo_2\{\mu$-$[(CO)_9Co_3(\mu_3$-$CCO_2)]\}_4$: Freshly prepared crystalline $(CO)_9Co_3(\mu_3$-$CCOOH)$ (0.243 g, 0.500 mmol) and $Mo_2(CH_3CO_2)_4$ (0.0357 g, 0.0833 mmol) were loaded as above and 80 mL of 1:1 (v:v) THF/toluene was added to the flask through syringe with rapid stirring. After 18 h reaction at room temperature the reaction mixture was cooled to −40 °C. The solid material in the reaction mixture was collected by filtration and washed with 2 × 5 mL of toluene. The black-blue powdery material from the filtration was then pumped to dryness and characterized as $Mo_2\{\mu$-$[(CO)_9Co_3(\mu_3$-$CCO_2)]\}_4$ (0.106 g, 0.0500 mmol). The corresponding yield based on total molybdenum is 60%. Anal. Calcd for $Mo_2Co_{12}C_{44}O_{44}$: Co, 33.18; Mo, 9.00; C, 24.79; Found: Co, 33.34; Mo, 8.31; C, 23.03. IR (KBr, cm^{-1}, carbonyl and carboxylate regions) 2104s, 2080 s,sh, 2042 vs, 2121 s, 2011 s, 1453 w, 1357 m.

$Cu_2\{\mu$-$[(CO)_9Co_3(\mu_3$-$CCO_2)]\}_3[\mu$-$(CH_3CO_2)][OC_4H_8]_2$: $Cu(CH_3$-$COO)_2$·H_2O (0.4 mmol, 0.080 g) and $(CO)_9Co_3(\mu_3$-$CCOOH)$ (0.8 mmol, 0.388 g) were loaded into a 50 mL Schlenk flask equipped with a rubber septum and a magnetic stirring bar. This flask had been evacuated and refilled with dinitrogen several times before 25 mL of CH_2Cl_2 were added to the flask via syringe with rapid stirring. Stirring of the reaction mixture was continued for 20 h at room temperature to give a purple solution. CH_2Cl_2 was removed under vacuum and the residual red-dark powder was extracted by 20 mL of THF to give purple solution. THF was slowly removed under vacuum and the resulting dark-red microcrystals were extracted by hexane to give a red-purple solution. Finally hexane was removed under vacuum to yield 0.159 g of $Cu_2\{\mu$-$[(CO)_9Co_3(\mu_3$-$CCO_2)]\}_3[\mu$-$(CH_3CO_2)][OC_4H_8]_2$. The yield based on total copper was 44%. Anal. Calcd for $Cu_2Co_9O_{37}C_{43}H_{19}$: Cu, 7.12; Co, 29.71; C, 28.93; H, 1.07. Found: Cu, 7.48; Co, 29.96; C, 29.16; H, 1.00. IR (KBr, cm^{-1}, carbonyl and carboxylate regions) 2107 s, 2051 vs, br, 2044 vs, sh, 1598 m, 1434 w, 1374 m, 1338 w, sh.

A single crystal suitable for X-ray diffraction was obtained by the following procedure. $Cu_2\{\mu$-$[(CO)_9Co_3(\mu_3$-$CCO_2)]\}_3[\mu$-$(CH_3CO_2)][OC_4H_8]_2$ was dissolved in a mixed THF/hexane (1:1) solvent, and the resulting solution was kept at −20 °C for several days and then −40 °C for ≈2 weeks. The black needlelike crystals $Cu_2\{\mu$-$[(CO)_9Co_3(\mu_3$-$CCO_2)]\}_3[\mu$-$(CH_3CO_2)]$-$[OC_4H_8]_2$·0.5 THF were collected. The crystal was mounted with epoxy on the end of a glass fiber and data were collected with an Enraf-Nonius CAD4 diffractometer equipped with a graphite crystal monochromatic Mo Kα X-radiation source. The structure was solved by MULTAN direct methods followed by successive difference Fourier syntheses. Full-matrix least-squares refinements were employed. All non-hydrogen atoms were refined with anisotropic thermal parameters in the final cycles, except for the carbon atoms of coordinated THF and all atoms of solvated THF molecules. Relevant crystallographic information is summarized in Table 1 and the ORTEP diagram is given in Figure 1.

$Cu_2\{\mu$-$[(CO)_9Co_3(\mu_3$-$CCO_2)]\}_4$·2THF, $Cu(CH_3COO)_2$·H_2O (0.8 mmol, 0.160 g) and $(CO)_9Co_3(\mu_3$-$CCOOH)$ (1.6 mmol, 0.776 g) were loaded into a 100 mL Schlenk flask equipped with a rubber septum and a magnetic stirring bar. This flask had been evacuated and refilled with dinitrogen several times before 50 mL of CH_2Cl_2 was added to the flask via syringe with rapid stirring. After 20 h of additional stirring at room temperature, a purple solution with considerable precipitate was formed. CH_2Cl_2 was removed under vacuum and the residual dark-red powder was dissolved in 30 mL of THF and stirred for 15 h to give a purple solution. Then THF was slowly removed under vacuum, and the resulting dark-red microcrystals were washed by 30 mL of CH_2Cl_2 to give a great deal of red-brown precipitate and a purple solution. To the purple solution was added 30 mL of hexane. The resulting solution was stirred for a couple of hours to yield more red-brown precipitate. The precipitate was washed with hexane to give total of 0.70 g of $Cu_2\{\mu$-$[(CO)_9Co_3(\mu_3$-$CCO_2)]\}_4$·2THF. The yield based on total Co was 80%. Anal. Calcd for Cu_2 $Co_{12}O_{46}C_{52}H_{16}$: Cu, 5.75; Co, 31.99; C, 28.25; H, 0.73. Found: Cu, 5.81; Co, 32.13; C, 28.06; H, 0.74. IR (KBr, cm^{-1}, carbonyl and carboxylate regions) 2108 s, 2043 vs, 2022 s, 2012 s, 1574 w, 1365 m, 1338 w, sh.

Materials Characterization. In all the following experiments, care was taken not to expose the precursors to air. This was particularly important for the molybdenum precursor. The TGA measurements under different atmospheres were carried out in a Cahn Electrobalance. The sample was heated linearly from room temperature to 673 K in 190 min in flowing helium or hydrogen (100 mL/min, NPT). The electronics of the

(8) Cen, W.; Lindenfeld, P.; Fehlner, T. P. *J. Am. Chem. Soc.* **1992**, *114*, 5451.
(9) Kriz, O.; Rehingold, A. L.; Shang, M.; Fehlner, T. P. *Inorg. Chem.* **1994**, *33*, 3777.
(10) Cen, W.; Haller, K. J.; Fehlner, T. P. *Inorg. Chem.* **1993**, *32*, 995.

Table 1. Crystal Data for $Cu_2\{\mu\text{-}[(CO)_9Co_3(\mu_3\text{-}CCO_2)]\}_3[\mu\text{-}(CH_3CO_2)][OC_4H_8]_2\cdot 0.5THF$

empirical formula	$Cu_4Co_{18}O_{75}C_{90}H_{46}$
formula weight, dalton	3642.28
crystal dimensions, mm	0.30 × 0.10 × 0.08
crystal color/shape	dark red needles
temp, K	293
crystal system	monoclinic
space group	*C*2/*c* (No. 15)
a, Å	21.783(5)
b, Å	15.978(1)
c, Å	37.463(8)
β, deg	94.06(2)
V, Å^3	13006(7)
lattice parameter refinement	25 reflns; 24° < 2θ < 28°
Z	4
calcd density, g/cm^3	1.860
μ (Mo Kα), cm^{-1}	29.632
diffractometer	Enraf-Nonius CAD4
radiation	graphite-monochromated Mo Kα, λ = 0.710 73
attenuator	Zr foil, factor 19.291
takeoff angle, deg	2.8
detector aperture, mm	horizontal 1.65−2.10; vertical 4.0
crystal−detector distance, cm.	21
scan type	ω−2θ
scan rate, deg/min in ω	1.39 to 5.56
scan width, deg	0.55 + 0.35 tan θ
2θ range, deg	4.0 to 46.0
data total measured	9403
unique $F_o^2 > 3\sigma(F_o^2)$	5173
unique measured	7415
corrections, on *I*	Lorentz polarization nonlinear decay (0.9767−1.1804), ψ curve absorption (trans: 0.9568−0.9994)
reflection averaging	237 multiples, $R_{merg}(I) = 0.023$; $R_{merg}(F) = 0.020$
refinement	full-matrix least-squares
hydrogen atom	not included
minimization function	$\Sigma w(\|F_o\| - \|F_c\|)^2$
p, weight = $[\sigma^2(F^2) + p^2F^2]^{-1/2}$	0.04
anomalous dispersion	all non-hydrogen atoms
data: variable ratio	6.5
$R_1 = \Sigma\|\|F_o\| - \|F_c\|\|/\Sigma\|F_o\|$	0.0464
$R_2 = (\Sigma w(\|F_o\| - \|F_c\|)^2/\Sigma wF_o^2)^{1/2}$	0.0603
goodness of fit	1.68
convergence, largest shift/error	0.05
highest peak in final diff map, e/Å^3	0.693
lowest peak in final diff map, e/Å^3	−0.470
computer hardware	VAXstation 3200
computer software	SDP/VAX

electrobalance were purged with flowing argon. All the gases used were ultrahigh purity, and they were passed over traps to remove water.

To identify the nature of the species evolving from the molecular precursors during thermolysis, temperature programmed desorption−mass spectrometry (TPD-MS) analyses at atmospheric pressure were performed with a UTI-100-C quadrupole mass spectrometer equipped with a fast response continuous inlet system. Preliminary mass scans were carried out during the activation of the samples to determine the ion signals generated on heating the molecular precursors. On this basis, ions characteristic of CO, CO_2, CH_4, H_2O, hydrocarbons, and C_1 oxygenates were observed. The precursors were heated from 298 to 623 K in 45 min in flowing helium or hydrogen (100 mL/min). The evolution in time of the different ion signals was recorded as a function of the temperature of the sample being pyrolyzed. Only relative intensities were measured.

BET surface areas were measured with a Quantachrome unit at 77 K with nitrogen as the adsorbate and helium as the carrier gas. Materials were prepared in situ from the precursors by activation under helium and under flowing hydrogen.

X-ray photoelectron spectroscopic (XPS) measurements were conducted in a Kratos XSAM-800 spectrometer using a magnesium anode and equipped with a pretreatment chamber. Samples in the form of thin films were prepared by evaporating a concentrated solution of the corresponding molecular precursor in THF on the surface of gold-plated copper holders which were mounted on a heatable insertion probe. After a spectrum of the molecular precursor was obtained, the sample was converted into the catalytic solid material in the pretreatment chamber. Prior to any measurement, the pretreatment chamber was evacuated to 10^{-8} Torr and the sample was cooled down to room temperature. The sample was heated for 2 h at 373−423 and 573 K. The C1s, O1s, Co2p, Cu2p, and Mo3d ionization regions were analyzed. The reported binding energies (BE) are referenced to a C1s BE of 285.0 eV.

The evolution of the molecular precursors into the catalytic solids as a function of temperature during the activation in helium, hydrogen or the reaction mixture (2% 1,3-butadiene in H_2) was followed by means of in situ diffuse reflectance infrared spectroscopy (DRIFTS). The molecular precursor (≈5 mg) was mixed with KBr (≈85 mg, Aldrich) and placed in the sample holder of a diffuse reflectance reaction cell (Figure 2, Harrick Co.) in a FTIR spectrometer (Mattson, Galaxy-2000). All the infrared spectra are calculated in Kubelka−Munk−Shuster units,[11] for a system that scatters radiation[12] 416 scans were averaged at 4 cm^{-1} resolution. Each spectrum requires 4−5 min and the single-beam emissivity spectra are ratioed to pure KBr in equivalent conditions. Dilution in KBr also minimizes the effects of the volume decrease of the precursor on thermolysis so that the reflected signal remains focused into the detector during the whole experiment. In the DRIFTS cell gases flow through the sample from beneath it as the temperature is increased in a stepwise fashion by 10 K

(11) Kubelka, P. *J. Opt. Soc. Am.* **1948**, *38*, 448.
(12) Klier, K. In *ACS Symp. Ser.*; Comstock, M. J., Ed.; American Chemical Society: Washington, DC, 1980; Vol. 137, Chapter 8.

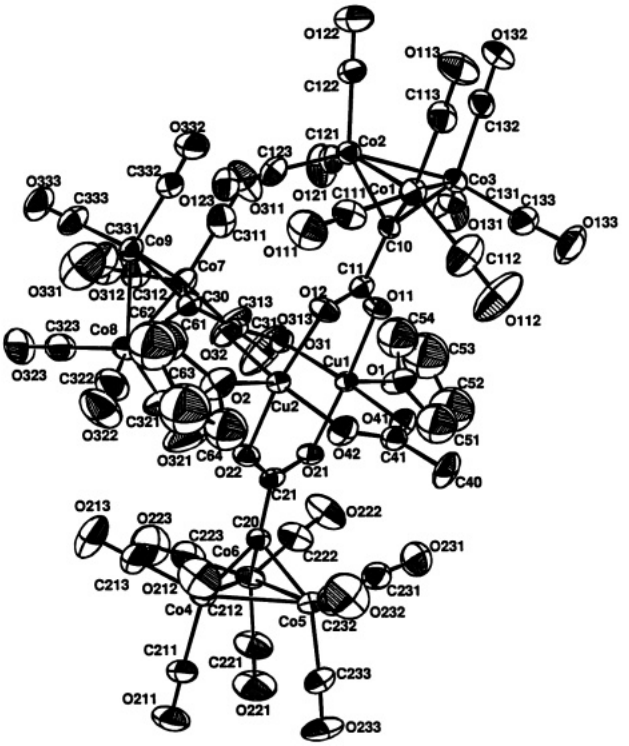

Figure 1. ORTEP diagram of $Cu_2\{\mu$-$[(CO)_9Co_3(\mu_3$-$CCO_2)]\}_3[\mu$-$(CH_3CO_2)][OC_4H_8]_2$ with thermal ellipses showing 40% probability. Bond distances and angles (supplementary material) are all within the ranges found for $Cu_2[\mu$-$(CH_3CO_2)]_4$ and $(CO)_9Co_3(\mu_3$-$CH_3)$, respectively.

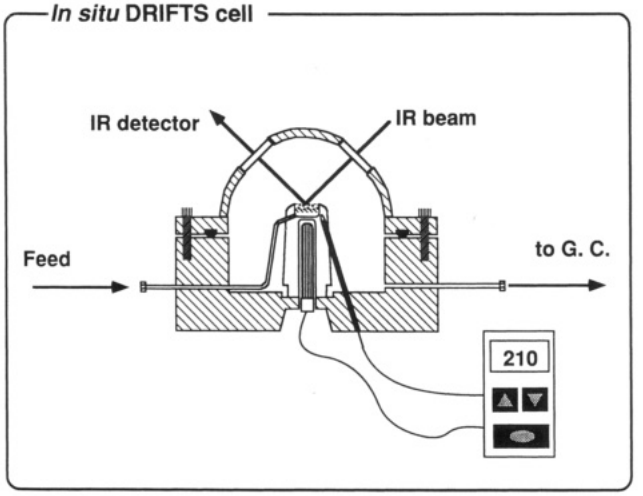

Figure 2. Schematic drawing of the in situ DRIFTS cell.

increments. The total flow for either helium, hydrogen, or the reaction mixture of 50 mL/min was chosen in order to keep the residence time similar to that in the flow microreactor (see below). The catalysts diluted in KBr show similar product selectivity but lower conversion compared to the undiluted catalysts in the flow microreactor.

Catalytic Activity. The system shown in Figure 3 was used to investigate the activities of the catalytic solids. Again the molecular precursors were transformed in situ into the catalysts by thermal activation in flowing helium, hydrogen, or the 1,3-butadiene plus hydrogen reaction mixture in a quartz flow microreactor (4 mm i.d.). Typically 16 mg of the specific molecular precursor was activated under the 2% 1,3-butadiene in H_2. After preparation of the catalyst, the hydrogenation reaction was run at atmospheric pressure in the temperature range 310−473 K. To do so, the prepared catalyst was fed with a reaction mixture of hydrogen:butadiene = 50:1 molar ratio at a total flow rate of 100 mL/min. The proportions of hydrogen and 1,3-butadiene were changed in the reaction feed to determine the reaction order of both

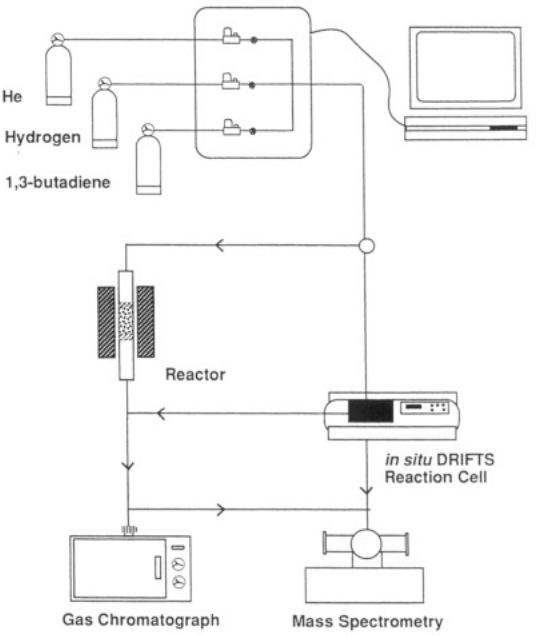

Figure 3. Schematic drawing of the microflow reaction system.

reactants. In these measurements helium was used to keep the total flow constant. Mass flows were controlled by flow controllers (Brooks, Model 5850-E), and the reaction system was under computer control. The reactor effluent was analyzed by gas chromatography on a Hewlett-Packard 5890-II GC provided with a FID detector. A picric acid packed column (6 ft × $^1/_8$ in.) supplied by Alltech was used to separate the effluents which were mainly 1-butene, *n*-butane, *cis*-2-butene and *trans*-2-butene. Hydrogenolysis products produced during activation were analyzed similarly in the same column.

Results and Discussion

Precursors. The geometric and spectroscopic data show that the tricobalt cluster acts as a ligand substituent formally replacing the methyl group in the metal acetate. That is, the fundamental structure and bonding of both the carboxylate and metal carbonyl cluster portions of the clusters of clusters are similar to those of the metal acetates[13] and tricobalt alkylidyne clusters, respectively.[14] On the other hand, the steric and electronic effects of the tricobalt substituent are very different from those of a typical organic group.[15] In the case of the Mo compounds, we have already commented on the unusual optical properties generated by the cluster substituents.[16] The present work shows that the unusual properties of the cluster substituent also are expressed in the synthetic chemistry as follows.

These clusters of clusters are synthesized by the facile exchange reaction of the metal acetate, $M_2(CH_3COO)_4$, with the cluster acid, $(CO)_9Co_3CCOOH$. The origin of the clean exchange reaction lies in the fact that the tricobalt cluster substituent makes $[(CO)_9Co_3CCOO]^-$ a better ligand than $[CH_3COO]^-$, i.e., $(CO)_9Co_3CCOOH$ is a weaker acid than CH_3COOH. For both Cu and Mo the exchange of the first three acetate ligands is fast, whereas that of the fourth is slow. This permits the

(13) Mehrotra, R. C.; Bohra, R. *Metal Carboxylates*; Academic Press: New York, 1983; p 396.
(14) Seyferth, D. *Adv. Organomet. Chem.* **1976**, *14*, 97.
(15) Worth, G. H.; Robinson, B. H.; Simpson, J. *J. Organomet. Chem.* **1990**, *387*, 337.
(16) Fehlner, T. P.; Calvo-Perez, V.; Cen, W. *J. Electron Spectrosc.* **1993**, *66*, 29.

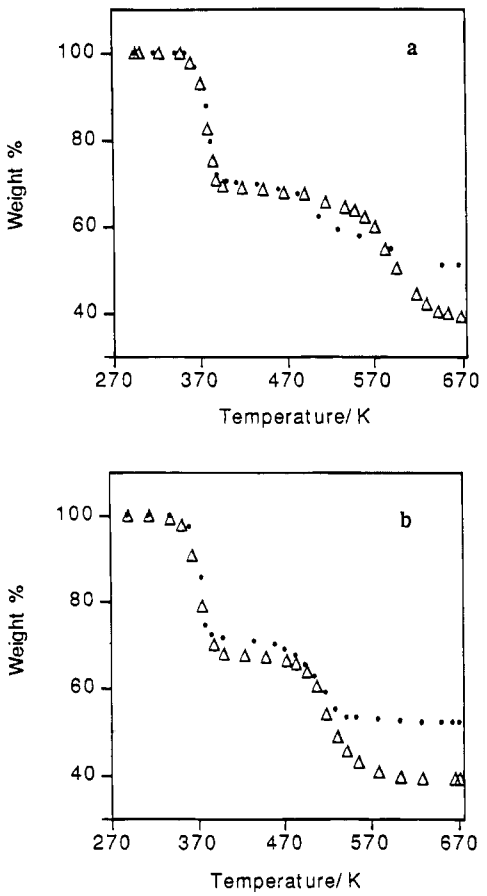

Figure 4. TGA analyses: (a) MoCo precursor; (b) CuCo precursor. Solid dots in He, open triangles in H_2.

Chart 2

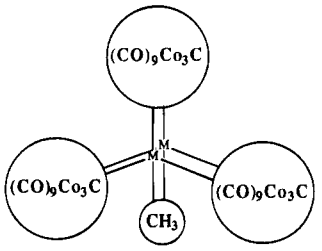

isolation of both soluble $M_2\{(CO)_9Co_3CCOO\}_3(CH_3COO)$ and insoluble $M_2\{(CO)_9Co_3CCOO\}_4$ forms in good yield. The first substitution product was crystallographically characterized for M = Cu (Figure 1) whereas the second was crystallographically characterized for M = Mo (as the soluble $Mo_2\{(CO)_9Co_3CCOO\}_4\{(CO)_9Co_3CCOOH\}_2$ adduct).[8] The relatively slow conversion of $M_2\{(CO)_9Co_3CCOO\}_3(CH_3COO)$ to $M_2\{(CO)_9Co_3CCOO\}_4$ can be ascribed to the steric requirements of the tricobalt cluster. This is illustrated nicely by the structure of $Cu_2\{(CO)_9Co_3CCOO\}_3(CH_3COO)$ where it is found that the large $(CO)_9Co_3CCOO$ cluster ligands are distinctly folded around toward the small CH_3COO ligand as schematically shown in Chart 2, thereby hindering entry of the fourth cluster acid.

Materials Characterization. Except for preliminary experiments, only the $M_2\{(CO)_9Co_3CCOO\}_4$ forms were used in the catalytic investigations. The TGA results are given in Figure 4. For both precursors a two step weight loss is observed. The first weight loss is ≈30% for both precursors in He and in H_2. However, the second differs depending on the atmosphere. In He it is ≈50% and in H_2 it is 60% which corresponds to a

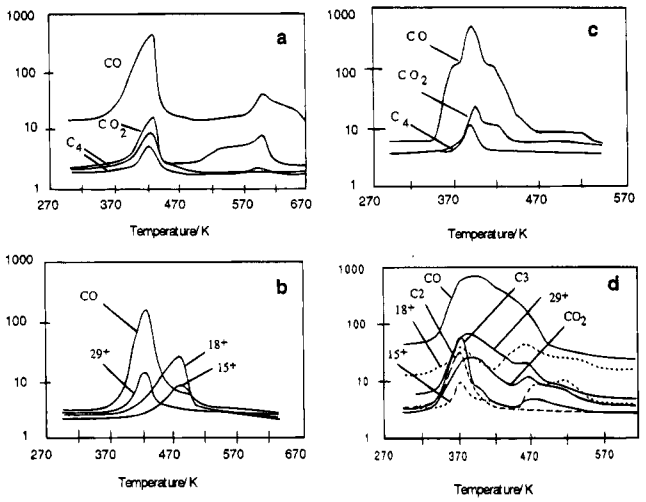

Figure 5. TPD–MS ion intensities in helium for the cobalt-based clusters of clusters: (a) MoCo–He; (b) MoCo–H_2; (c) CuCo–He; (d) CuCo–H_2.

Table 2. BET Surface Area

	MoCo		CuCo[a]	
treatment	helium	hydrogen	helium	hydrogen
2h/393 K	60	33	7	3
2h/493 K	125	54	22	10

[a] Prepared from $Cu_2\{\mu\text{-}[(CO)_9Co_3(\mu_3\text{-}CCO_2)]\}_3[\mu\text{-}(CH_3CO_2)][OC_4H_8]_2$.

residual composition of $M_2Co_{12}(CCO_2)_4$ and M_2Co_{12}, M = Mo, Cu, respectively. In the following, the metastable solid decomposition product produced at ≈400 K is designated LT-MCo and that produced above 500 K is designated HT-MCo.

Examination of the TPD-MS profiles (Figure 5) permits the identification of the principal gaseous products formed during the decomposition. Under He, it is seen that the first TGA weight loss is associated with CO evolution but ions attributed to CO_2 and solvent (coordinated THF in the case of CuCo and residual solvent in the case of MoCo) are observed as well. The maximum in gas production occurs at approximately the same temperature as the first mass loss in the tga. Under He, smaller amounts of CO and CO_2 evolution at 520–620 K is evident in the second stage of the formation of MoCo. No second maximum is observed for CuCo, however, and the evolution of CO and CO_2 appears continuous. The TPD-MS results under H_2 show that the presence of H_2 facilitates the ligand loss. Although CO is still the principal product, significant ion signals at *m/e* 15, 29, 18, and 43 suggest the formation of C_1-oxygenates, water, and hydrocarbons with CO_2 formation less prominent. Again, the first maximum in gas production corresponds well with the first mass loss in the TGA but the second weight loss is poorly reproduced at best. The TGA and TPD-MS results together establish that the rupture of Co–CO bonds is the primary initial decomposition pathway. Under an H_2 atmosphere (or the reaction mixture) the hydrogenolysis of the carboxylate links apparently takes place.

The surface areas were measured for materials produced at 393 and 493 K under He as well as under H_2. The results are given in Table 2 where it will be seen that there are large differences between the materials. The surface areas roughly double in going from materials prepared in H_2 relative to those in He. In addition

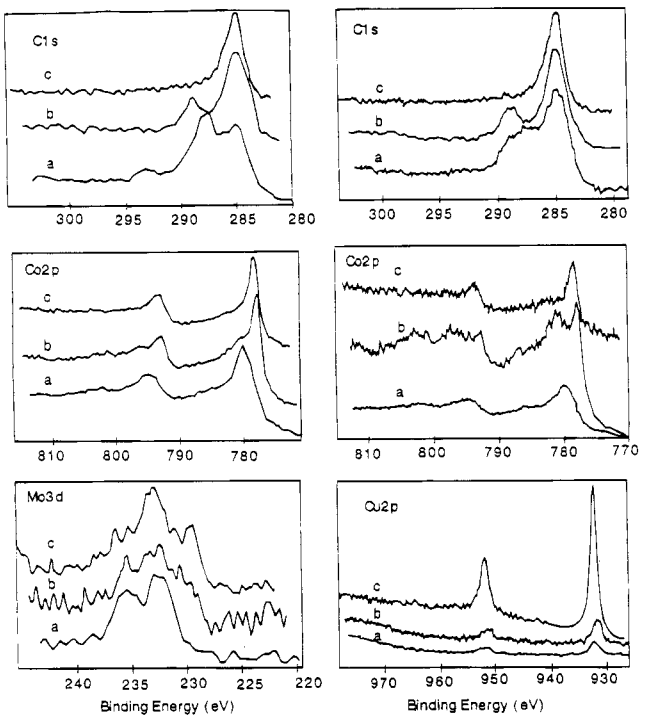

Figure 6. XPS: left, MoCo precursor; right, CuCo precursor. (a) Unheated, (b) heated at 393 K in vacuum for 2 h, and (c) heated at 593 K in vacuum for 2 h.

the surface areas are much smaller for CuCo than for MoCo. The latter are about half those observed previously for CoCo and ZnCo.[5] Note that the surface area of HT-MoCo falls to 15 m^2/g after exposure to air.

The XPS measurements for the precursors and the LT- and HT-MCo, M = Mo and Cu, films are presented in Figure 6. For the molecular precursors the second carbon ionization at ca. 290 eV is due to the carbon associated with the carbonyl and carboxylate ligands. The intensity of this band decreases after heating at 393 K but, consistent with the tga and tpd-ms results, does not disappear until the highest temperature is achieved. The 795 (Co $p_{1/2}$) and 780 (Co $p_{3/2}$) eV ionizations of the precursor shift ≈2 eV to lower binding energy on heating indicating the formation of cobalt metal. Note that there is still a significant fraction of ligand-bound cobalt in the LT-CuCo material as evidenced by the two Co ionizations (Figure 6). This is consistent with the two-step decomposition process discussed above.

The XPS measurements on the core metals are less informative. The signal to noise for the Mo $3d_{3/2}$, Mo $3d_{5/2}$ ionizations is poor although there is a suggestion of partial reduction of the metal on heating which is consistent with loss of some of the carboxylate−Mo(II) links in the solid. For the Cu $2p_{1/2}$ Cu $2p_{3/2}$ signals, no significant change in binding energy is observed on heating; however, there is a significant increase in intensity relative to the cobalt signals at the highest temperature. This suggests an enrichment of the surface with copper and substantial rearrangement of the material at these temperatures. No evidence for a similar migration of Mo to the surface is observed.

The in situ infrared spectra measured during the preparation of MoCo and CuCo are presented in Figure 7. Three regions are of importance. The CO terminal stretching vibrations (2100−1900 cm^{-1}) are associated with the $(CO)_9Co_3C-$ cluster substituents. The carboxylate symmetric and antisymmetric stretching modes (1600−1350 cm^{-1}) are associated with the external cluster−internal cluster carboxylate links. Finally, for the spectra obtained in the presence of the reaction mixture, the CH stretching vibrations (3000−2900 cm^{-1}) are associated with hydrocarbon moieties on the surface.

There are qualitative similarities in the changes observed in the carbonyl and carboxylate regions for heating the precursors under He, H_2, or the reaction mixture. Most importantly, the carbonyl bands disappear at lower temperatures than do the carboxylate bands. Consistent with the results already presented, this shows definitively that the Co−CO links are broken before the carboxylate links. In turn, this suggests that the core bonding of the cluster of clusters is mainly preserved in some form during the loss of Co−CO bonds and the formation of Co−Co bonds. The latter is established by the XPS results.

A more detailed analysis of these regions provides a closer look at the manner in which the MCo solids are formed. In the carbonyl region, the sharp band at 2108 cm^{-1}, which is characteristic of the intact $(CO)_9Co_3C-$ clusters, decreases on heating. This is accompanied by an increase and then decrease in a band at 1870 cm^{-1} which is characteristic of bridging carbonyls (Figure 8). Loss of terminal Co−CO ligands results in unsaturated metal centers which may promote the formation bridging intra- or intercluster Co−C(O)−Co interactions. When the bands characteristic of intact $(CO)_9Co_3C-$ clusters and the intermediate species with bridging CO ligands have disappeared, a broad absorption at ≈1940 cm^{-1} remains. The frequency and intensity of this band decrease with increasing temperature, a situation reminiscent of the absorptions produced by CO absorbed on small metal particles. Here, too, the band maximum shifts to lower wavenumbers with decreasing coverage.[17] These observations suggest that cluster of clusters degradation begins with CO ligand loss from the tricobalt clusters. Cobalt atom aggregation takes place via an intermediary containing bridging CO ligands and the tiny particles continuously lose coordinated CO until the surface is bare. At this point the surface exhibits an XPS signal characteristic of cobalt metal.

The loss in metal carbonyl band intensity is accompanied by a broadening of the bands in the carboxylate region suggesting a perturbation of the carboxylate linkages. The difference between the symmetric and antisymmetric stretching frequencies varies considerably as the nature of the carboxylate coordination changes.[13] This suggests that loss of the tricobalt clusters is accompanied by the rearrangement of the carboxylate bonding. Although it is clear that carboxylate linkages of some type remain after all the CO ligands are lost, it is unlikely that the simple core structures found in the cluster of clusters precursors are the exclusive bonding mode.

In the carbonyl and carboxylate regions the infrared observations with the three different gaseous environments and two different core metals are essentially the same. Thus, although it is clear from the tga and tpd-ms experiments that the precursor reaction chemistry is different in He vs H_2, the net dynamic changes in the solid material as revealed by infrared measurements are very similar. There are some quantitative differences

(17) Sheppart, N.; Nguyen, T. T. *Adv. Infrared Raman Spectrosc.* **1978**, *5*, 67.

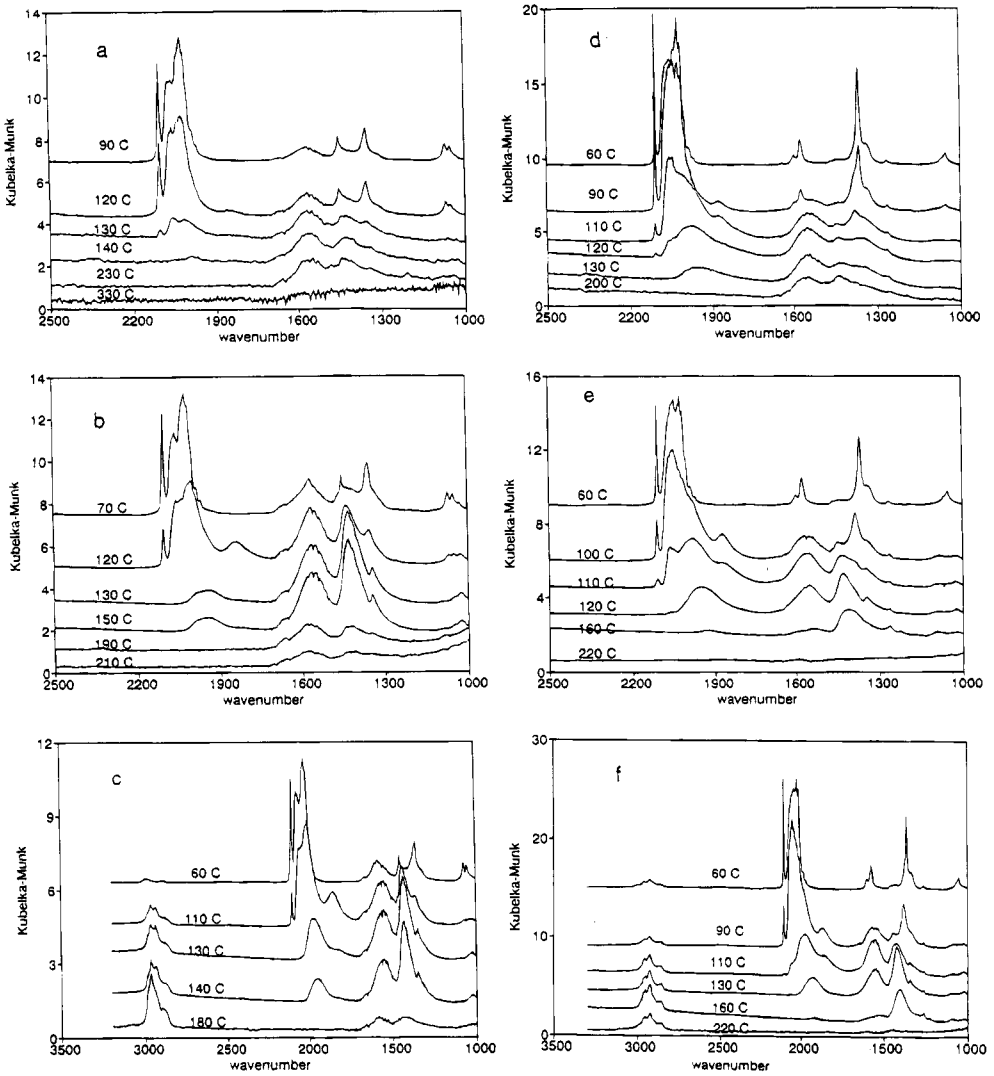

Figure 7. In situ DRIFTS during heating of MoCo precursor in (a) helium, (b) hydrogen, and (c) reaction mixture (butadiene/hydrogen); CuCo precursor in (d) helium, (e) hydrogen, and (f) butadiene/hydrogen.

Table 3. In Situ DRIFTS on the Preparation of MCo, M = Mo, Cu, from Clusters of Clusters Precursors

precursor	activation feed	bridge/linear carbonyl[a]	T(carbonyl)[b] (K)	T(carboxylate)[b] (K)
MoCo	He	0.2	463	583
	hydrogen	1.0	443	493
	C4H6/H2	1.1	433	493
CuCo	He	0.7	453	513
	hydrogen	0.8	453	473
	C4H6/H2	0.8	453	493

[a] Ratio of the maximum area of the infrared band at ca. 2108 cm^{-1} and the maximum area observed for the band of the bridging carbonyl species. [b] Maximum temperature where infrared bands for carbonyl or carboxylate species are observed.

in relative intensities and peak positions, and some of the former differences are illustrated in Table 3.

On the basis of the data in Figure 7, infrared analyses were carried out on samples heated for several hours in H_2 at temperatures high enough to eliminate the carbonyl ligands (373–400 K, LT-MCo) but below the temperatures required to eliminate all of the carboxylate ligands (>473 K, HT-MCo). These long-time infrared experiments showed that the carboxylate bands remained in the LT-MCo samples thereby justifying the designation of two material structures.

Note that the tga, tpd-ms, and IR observations were time dependent, whereas heating times for the BET and XPS experiments were sufficiently long (2–4 h) to achieve a steady-state behavior, i.e., the temperatures in the two types of experiments are not directly comparable. The TGA results for the two precursors are deceptively similar and can be interpreted only in light of the other experiments. The TPD-MS experiments show that CO loss is the major pathway but a complex mixture of gaseous products, including CO_2, results with a H_2 atmosphere. The surface areas also show a large difference between MoCo and CuCo. If large surface areas are associated with a supporting structure derived from the core, as we have argued previously,[5] then MoCo has less such structure than CoCo or ZnCo and CuCo has essentially none. The infrared measurements show definitively that the Co–CO bonds are broken before the carboxylate links are broken and support a two-step process for both precursors. The evolution of the solids as viewed by infrared is similar for MoCo and CuCo despite the different gas-phase reaction product behaviors and surface areas.

To summarize, although the structures of these amorpous materials are unknown, the spectroscopic data suggest that the LT materials are made up of partially decarbonylated precursors. Thus, we envison a porous network constructed of of disk-shaped $M_2\{(CO)_x$-$Co_3CCOO\}_4$, $x < 9$, building blocks. The typical activation in H_2 under HT conditions destroys the carboxylate

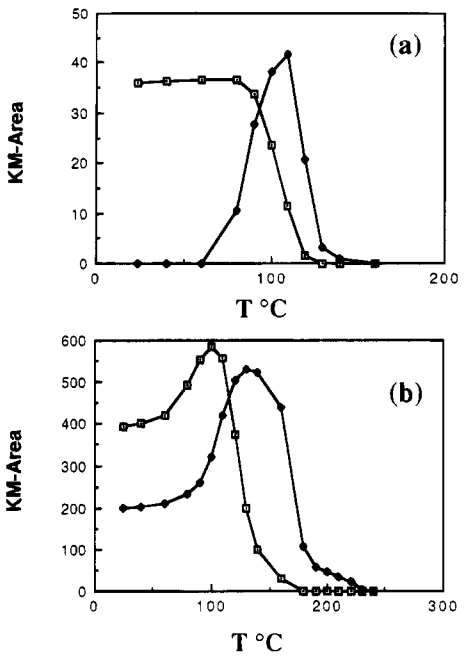

Figure 8. In situ DRIFTS intensities from heating $Mo_2\{\mu$-$[(CO)_9Co_3(\mu_3$-$CCO_2)]\}_4$ in the reaction mixture as a function of temperature: (a) the 2104 cm^{-1} band areas (open squares) and the 1860 cm^{-1} band areas (closed diamonds). (b) the sum of the carbonyl (open squares) and carboxylate (closed diamonds) band areas (the apparent increase in intensity is an artifact due to the difficulty of integrating the broad bands).

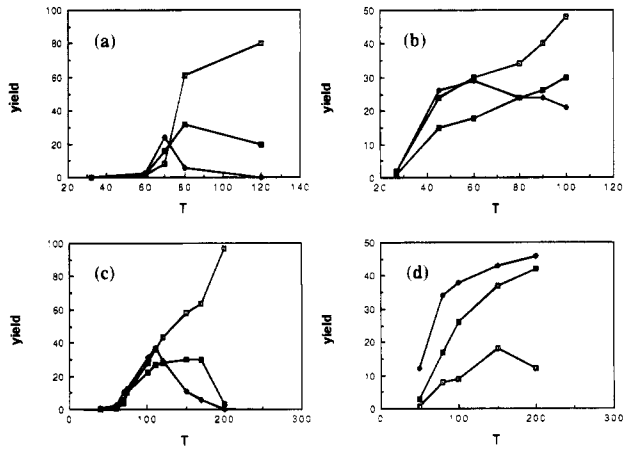

Figure 9. Yields of butane, 1-butenes, and 2-butenes vs reaction temperature: (a) LT-MoCo, (b) LT-CuCo (c) HT-MoCo, (d) HT-CuCo. Reaction feed: 100 H_2 + 2 mL/min 1,3-butadiene (open squares = butane, bold open squares = 2-butenes, closed diamonds = 1-butene).

core structure and we envision the formation of a metal, spongelike material which is more robust in the case of M = Mo than Cu. However, despite a lack of knowledge of precise structure, the significant, reproducible catalytic activity detailed in the following makes these materials interesting, new model systems.

Catalytic Activity. The hydrogenation of 1,3-butadiene yields mainly 1-butene, butane, *trans*-2-butene, and *cis*-2-butene as shown in Figure 9. In all cases, the selectivities for 1-butene and *n*-butane display a complementary behavior. However, the selectivities for 2-butenes are independent of the extent of 1,3-butadiene conversion and the accompanying changes in selectivity to *n*-butane and 1-butene.

No significant differences for 1,3-butadiene hydrogenation are observed in the case of the LT series. In the two LT-catalysts *n*-butane and 1-butene show complementary selectivity trends. The selectivity ratio 1-butene/*n*-butane are higher or close to unity and at conversions above ca. 80% butane becomes the most important hydrogenation product. The selectivities to 2-butenes do not appear to be significantly affected by the conversion level of butadiene. The carboxylate moieties which hold this structure are stable under reaction conditions below ca. 430 K for several hours. Most of the experiments for the LT samples were run at significantly lower temperatures (typically 313–373 K) ensuring the stability of the LT structure. Under these conditions not only does the second metal stays in the inner layer, but also there is no direct metal–metal bonding between the cobalt and the core metal atoms. The binding between the two metal layers is through the carboxylate ligands which may attenuate electronic effects from the second metal. Conversely, selectivity differences are observed for the butadiene hydrogenation activity when carboxylate ligands are removed from the catalyst structure. The HT-CuCo material is selective for 1-butene formation through all the conversion range, whereas HT-MoCo is selective for butane.

Selectivity trends were also observed in the product stream of the DRIFTS reaction cell during the preparation of the MCo materials in the reaction mixture. These indicate that 1-butene is the main hydrogenation product as long as significant amounts of the $(CO)_9Co_3C$– cluster is present. As the broad CO band at 1940 cm^{-1} disappears, the selectivity for complete hydrogenation increases. The higher the temperature, the more rapid is the change in selectivity to the steady state. Long-time experiments showed modest stabilities for the catalysts. For example, HT-MoCo showed reproducible temperature-up, temperature-down behavior, and the yield of 1-butene fluctuated 15% over 400 min at 353 K.

The reaction order for hydrogen was always approximately 1 and that for 1,3-butadiene approximately 0. Similar orders have been observed in other catalytic systems for the same reaction[18,19] and strongly suggest that the surface is saturated with the adsorbed hydrocarbon. The products formed during the reaction should be related to the predominant adsorbed species during the reaction.[20] Thus, the infrared bands of the adsorbed alkyl species provides some information on the nature of these adsorbed species. In fact, in situ infrared spectra provide evidence for the presence of adsorbed hydrocarbon species. As shown in Figure 7, infrared bands are observed at 2965, 2935, 2877, and 2862 cm^{-1}. These bands are characteristic of aliphatic C–H vibrations.[21-23] The infrared bands located at 2965 and 2935 cm^{-1} (antisymmetric C–H vibrational modes of the methyl and methylene groups) are clearly observed and their intensities can be measured. As *n*-butane and the isomers of butene are the only hydrogenation products, these absorptions are derived from four carbon atom linear hydrocarbons. Further, the complementary selectivities of *n*-butane and 1-butene shows that the

(18) Pradier, C. M.; Margot, E.; Berthier, Y.; Oudar, J. *Appl. Catal.* **1988**, *43*, 177.
(19) Pradier, C.-M.; Berthier, Y. *J. Catal.* **1991**, *129*, 356.
(20) Sautet, P.; Paul, J. F. *Catal. Lett.* **1991**, *9*, 245.
(21) Morrow, B. A.; Sheppard, N. *Proc. R. Soc. London, Ser. A* **1969**, *311*,
(22) Campione, T. J.; Ekerdt, J. G. *J. Catal.* **1986**, *102*, 64.
(23) Anderson, K. G.; Ederdt, J. G. *J. Catal.* **1989**, *116*, 556.

former results from the hydrogenation of 1-butene. In fact, there is a direct relationship between the increase in $I(2965\ cm^{-1})/I(2935\ cm^{-1})$ and the selectivity of *n*-butane, i.e., the higher the concentration of alkyl-like surface species the greater the selectivity toward *n*-butane.

The major difference between MoCo and CuCo as catalysts is the greater yield of 1-butene for the latter at all temperatures (conversion). One factor that may be responsible for the difference in selectivity is the low surface area of CuCo vs MoCo. That is, the difference in selectivity can be caused by the lower hydrogenation activity of CuCo. In turn, the lower surface area and activity of CuCo is attributed to the lack of M–M bonding in the precursor core. The other factor that becomes important at high conversion is the nature of the second metal. The XPS analysis indicates that Cu migrates to the surface whereas Mo does not. It is known that the existence of a mixed metal environment can affect the interaction of the adsorbates with the surface. That is, the presence of electron donors is reported to increase the selectivity to partial hydrogenation[24] as is the case of nitrogen bases[3,25,26] by decreasing the strength of the adsorption of the hydrocarbon.

(24) Sarkany, A.; Zsoldos, Z.; Furlong, B.; Hightower, J. W.; Guczi, L. *J. Catal.* **1993**, *141*, 566.
(25) Boitiaux, J. P.; Cosyns, J.; Martino, G. In *Metal Support and Metal Additivie Effects in Catalysis*; Imelik, B., Ed.; Elsevier: Amsterdam, 1982; p 355.
(26) Boitiaux, J. P.; Cosyns, J.; Vasudevan, S. *Appl. Catal.* **1985**, *15*, 317.

Conclusions

The molecular complexes, $M_2\{\mu\text{-}[(CO)_9Co_3(\mu_3\text{-}CCO_2)]\}_4$, M = Mo, Cu, can be converted by thermolysis into active heterogeneous catalysts for the hydrogenation of 1,3-butadiene. Two distinct forms of the catalysts can be prepared. The first, prepared at 400 K (LT-MCo), is partially decarbonylated and retains metal carboxylate linkages. The second, formed at 500 K (HT-MCo), is fully decarbonylated and, under H_2, fully decarboxylated. These catalysts differ structurally from those prepared from precursors with an octahedral array of tricobalt clusters and oxocarboxylate cores. Significant differences in the catalytic activities and selectivities result and these are also different from those exhibited by the ZnCo and CoCo materials studied earlier. These results demonstrate a dependence of catalytic behavior on molecular precursor core structure.

Acknowledgment. The present work was supported by the National Science Foundation CHE91-06933. The authors gratefully acknowledge Mr. Patrick Pinhero for his aid with the XPS experiments.

Supplementary Material Available: Crystal data, atomic positional and displacement parameters, and selected distances and bond angles for $Cu_2\{\mu\text{-}[(CO)_9Co_3(\mu_3\text{-}CCO_2)]\}_3[\mu\text{-}(CH_3CO_2)][OC_4H_8]_2\cdot 0.5$ THF, (17 pages). Ordering information is given on any current masthead page.

CM940460P